Bioactive Materials 46 (2025) 423–433

Contents lists available at ScienceDirect

Bioactive Materials

journal homepage: www.keaipublishing.com/en/journals/bioactive-materials

Multivalent ionizable lipid-polypeptides for tumor-confined mRNA transfection

Xiaofei Zhao, Yueyue Zhang, Xin Wang, Ziming Fu, Zhiyuan Zhong **, Chao Deng *

Biomedical Polymers Laboratory, and Jiangsu Key Laboratory of Advanced Functional Polymers, College of Chemistry, Chemical Engineering and Materials Science, State Key Laboratory of Radiation Medicine and Protection, Soochow University, Suzhou, 215123, China

ARTICLE INFO

Keywords:
mRNA delivery
Lipid-polypeptides
Multivalent interactions
Tumor-selective transfection
Cancer immunotherapy

ABSTRACT

mRNA therapeutics is revolutionizing the treatment concepts toward many diseases including cancer. The potential of mRNA is, however, frequently limited by modest control over site of transfection. Here, we have explored a library of multivalent ionizable lipid-polypeptides (MILP) to achieve robust mRNA complexation and tumor-confined transfection. Leveraging the multivalent electrostatic, hydrophobic, and H-bond interactions, MILP efficiently packs both mRNA and plasmid DNA into sub-80 nm nanoparticles that are stable against lyophilization and long-term storage. The best MILP@mRNA complexes afford 8-fold more cellular uptake than SM-102 lipid nanoparticle formulation (SM-102 LNP), efficient endosomal disruption, and high transfection in different cells. Interestingly, MILP@mLuc displays exclusive tumor residence and distribution via multivalency-directed strong affinity and transcytosis, and affords specific protein expression in tumor cells and macrophages at tumor sites following intratumoral injection, in sharp contrast to the indiscriminate distribution and transfection in main organs of SM-102 LNP. Notably, MILP@mIL-12 with specific and efficient cytokine expression generates significant remodeling of tumor immunoenvironments and remarkable antitumor response in subcutaneous Lewis lung carcinoma and 4T1 tumor xenografts. MILP provides a unique strategy to site-specific transfection that may greatly broaden the applications of mRNA.

1. Introduction

Messenger ribonucleic acid (mRNA) allows the rapid production of diverse proteins including cytokines, antibodies, antigens, genome-editing proteins, and thus holds immense potential to prevent and treat various diseases [1–4]. To date, two mRNA-based COVID-19 vaccines, BNT162b2 and mRNA-1273, have been approved by FDA, and over 1000 clinical trials of mRNA therapies have been conducted [5]. The application of mRNA therapies is heavily dependent on the rational design of delivery systems to protect mRNA from degradation and to overcome physiological barriers for effectual protein expression in desired cells [6–9]. Although lipid nanoparticles (LNP) have immensely contributed to the rapid development of mRNA drugs [10], liver enrichment and nonselective delivery considerably compromise therapeutic efficacy and induce off-target toxicities like hepatitis and liver injury [11–14].

Different strategies have been employed to accomplish non-liver delivery of mRNA drugs by LNP, such as optimizing ionizable lipids with amide and ester bonds in the tails [15–18], introducing the fifth component of selective organ targeting molecules (SORT) into LNP [19–21], and modifying the surface of LNP with targeting moieties [22–24]. Besides LNP, cationic polymers including poly(*β*-amino ester)s (PBAE) [25,26], charge-altering releasable transporters (CART) [27], polyaspartamide [28], and poly(TPAE-*co*-suberoyl chloride) have been developed for extrahepatic delivery of mRNA [29], affording selective protein expression in the lung and spleen by the introduction of PEG-lipid, tuning the charge ratios of mRNA to polymers as well as the alkyl chain length and molar ratios. Local-regional drug delivery especially intratumoral administration affords the potential to bypass physiological barriers, increase efficacy while concomitantly reduce off-target toxicity, and has emerged as a prominent modality for tumor treatment [30,31]. Following intratumoral administration, nanovehicles based on LNP and PBAE were reported to facilely deliver mRNA encoding IL-12, IL-15, and 4-1BBL, generating high level of protein expression, immune cell recruitment, and antitumor immunity at tumor sites [32,33]. Despite these local delivery systems elegantly increased

* Corresponding author.
** Corresponding author.
E-mail addresses: zyzhong@suda.edu.cn (Z. Zhong), cdeng@suda.edu.cn (C. Deng).

https://doi.org/10.1016/j.bioactmat.2024.12.032
Received 22 August 2024; Received in revised form 25 November 2024; Accepted 28 December 2024

the local mRNA concentrations and induced improved efficacy, the discernible distribution of mRNA and vehicles as well as protein expression in main organs might inevitably compromise their clinical applications [12]. Thus, delivery systems that enable exclusive distribution and protein expression of mRNA drugs in tumors are urgently required.

In this contribution, we have developed a series of multivalent ionizable lipid-polypeptides (MILP) to achieve robust mRNA complexation and tumor-confined transfection (Scheme 1). MILP can be developed through one-step aminolysis of poly(β-benzyl L-aspartate) with small molecules bearing alkanes (Cx) and tertiary amines (Ny), and its hydrophobicity, pK_a, and functionalities can be adjusted by changing the structure, length, and ratios of selected alkanes and tertiary amines. Polypeptides with outstanding biocompatibility, versatile structure and functionalities have received substantial attention for drug delivery and regenerative medicine [34–37]. Leveraging the multivalent electrostatic, hydrophobic, and H-bond interactions, MILP alone could provide robust affinity for mRNA complexation, cell binding, endosomal disruption, tumor residence and distribution. In mice bearing subcutaneous tumor xenografts, MILP@mRNA induced exclusive mRNA distribution and IL-12 expression at tumor sites, affording significant remodeling of tumor immunoenvironment and remarkable antitumor response.

2. Results

2.1. MILP development and mRNA complexation

MILP was obtained through one-step aminolysis of poly(β-benzyl-L-aspartate) (PBLA) with small molecules bearing linear/cyclic tertiary amines (Ny) and alkanes (Cx), termed as P(zCxNy) where z represents alkane mole fractions. PBLA was prepared with a degree of polymerization (DP) of 31 and narrow distribution ($M_w/M_n = 1.11$) by controlled polymerization of β-benzyl-L-aspartate *N*-carboxyanhydride (BLA-NCA) (Fig. 1A), as characterized by ^{1}H NMR, GPC, and MALDI-TOF measurements (Fig. S1). Fig. 1A showed the structures of Ny and Cx, with which 13 MILP compounds with z = 0.4 and 0.6 were prepared (Table S1). The complete disappearance of proton signal at 7.3 ppm attributed to benzyl groups, and the clear presentation of characteristic signals at 0.9–1.7 ppm in ^{1}H NMR spectra corroborated the successful construction of P(zCxNy) polypeptides (Figs. S2 and S3). mRNA complexation with MILP could be simply accomplished in sodium acetate buffer (AcNa, pH 4.0) via simple vortex (Fig. 1B), and the formed MILP@mRNA presented average diameter of sub-80 nm and positive zeta potential (Fig. 1C). Specifically, MILP@mRNA formed from P(0.6C8cN6M) (denoted as MILP11@mGFP) displayed a small size of about 60 nm, monodispersity, and spherical morphology as evaluated by DLS and TEM measurement (Fig. 1D and E). The mRNA encapsulation efficiency was approximately 90 % (Fig. S4), possibly due to the strong multivalent interactions of lipid-polypeptides with mRNA. As shown in Fig. 1F, the addition of Tween 20, NaCl, or urea caused gradual size increase of MILP11@mRNA, and the combined agents generated a size change of over ten times (Fig. 1F), possibly owing to the occurrence of hydrophobic (Tween 20), ionic (NaCl), and hydrogen bond (urea) interactions during complexation. On the contrary, the mRNA complex formed from P(N6-1) (P(N6-1)@mGFP) pending a tertiary amine showed larger average diameter of 276 nm (Fig. S5). Besides, isothermal titration calorimetry (ITC) measurements displayed that the binding constants (Ka) of P(0.6C8cN6M) were much higher than those of P(N6M) (Ka1: 4.2×10^8 vs 1.0×10^8; Ka2: 2.9×10^6 vs 2.4×10^5) (Fig. S6, Table S2), indicating the possible occurrence of multiple strong interactions between P(0.6C8cN6M) and mRNA. In addition, circular

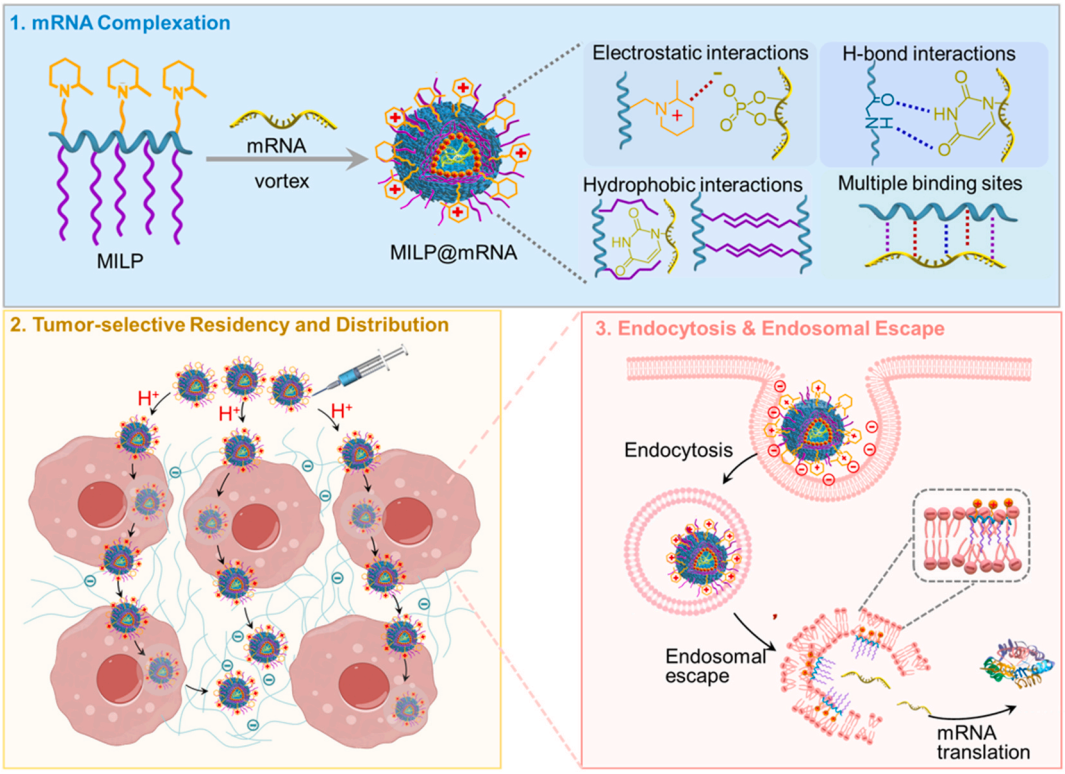

Scheme 1. Illustration of multivalent ionizable lipid-polypeptides (MILP) exploited to achieve robust mRNA complexation and tumor-confined transfection. Leveraging the multivalent electrostatic, hydrophobic, and H-bond interactions, MILP robustly packs mRNA into sub-100 nm MILP@mRNA nanoparticles. Under mild acidic tumor microenvironment (TME), MILP@mRNA was partially protonated and revealed exclusive tumor residence and distribution via multivalency-directed strong affinity and transcytosis. Subsequently, efficient endocytosis and endosomal escape of MILP@mRNA were achieved via multivalent perturbation of cell and endosome membranes, affording potent mRNA transfection.

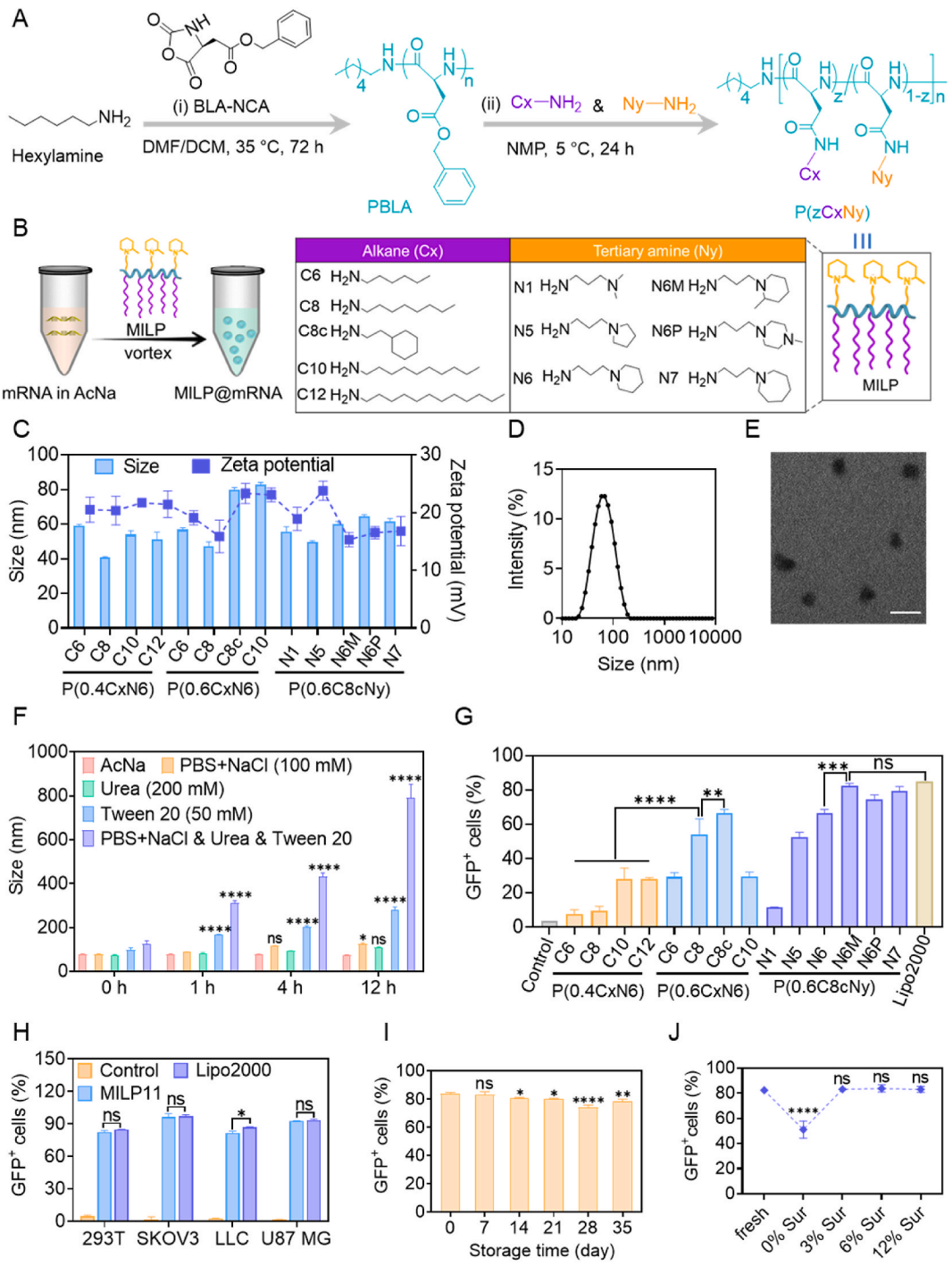

Fig. 1. Construction and characterization of multivalent ionizable lipid-polypeptides (MILP) complexed with mRNA (MILP@mRNA). (A) Synthesis route of lipid-polypeptides, and structures of small molecules bearing alkanes and tertiary amines for the synthesis of P(zCxNy), where "z" (0.4, 0.6) represents alkane (Cx) mole fractions. (B) Complexation of MILP with mRNA (MILP@mRNA). (C) Size and zeta potential of MILP@mGFP determined by dynamic light scattering (n = 3). (D) Representative size distribution and (E) TEM image of MILP11@mGFP formed from P(0.6C8cN6M). Scale bar, 100 nm. (F) Size variation of MILP11@mRNA in different solutions, control (AcNa buffer, 5 mM), PBS + NaCl (200 mM), urea (200 mM), Tween 20 (5 mM) and mixed solution (PBS + NaCl, urea and Tween 20) at 37 °C (n = 3). (G) Percentage of GFP$^+$ 293T cells following the treatment with MILP@mGFP for 24 h (mGFP: 1.0 μg/mL, n = 3). (H) Transfection efficiency of MILP11@mGFP and Lipo2000@mGFP in different cells at 24 h (mGFP: 1.0 μg/mL, n = 3). (I–J) Stability of MILP11@mGFP against storage at 4 °C (I) and lyophilization using sucrose (Sur, 3–12 %, w/v) as a protectant (J) as indicated by EGFP expression in 293T cells (mGFP: 1.0 μg/mL, n = 3). Statistical significance in (F, G, H, I and J) was analyzed by one-way ANOVA with Tukey's multiple comparisons test. (ns, not significant; *$p < 0.05$, **$p < 0.01$, ***$p < 0.001$, ****$p < 0.0001$).

dichroism (CD) spectra showed that P(0.6C8cN6M) adopted an α-helix structure (Fig. S7), which was reported to facilitate the stable complexation with nucleic acids [38]. In contrast with little size change of MILP@mRNA in PB within 12 h, the polyplexes treated with proteinase K (12.0 units/mL) displayed obvious swelling with an average sizes of around 600 nm at 12 h (Fig. S8), signifying their enzymatic degradability.

2.2. In vitro screening of MILP

293T cells were employed to evaluate the transfection efficiency of MILP complexed with mRNA encoding green fluorescent protein (MILP@mGFP). Confocal microscopy imaging (Fig. S9) and flow cytometry (Fig. 1G) analysis demonstrated that increasing the proportion of alkanes benefited the transfection efficiency, in which most of P (0.6CxNy) with an alkane mole fraction of 0.6 exhibited over 60 % GFP^+ cells, in sharp contrast with the low transfection efficiency (<30 %) in P (0.4CxNy) groups. Although elevated GFP expression was acquired by increasing the chain length of alkanes from C8 to C12 in P(0.4CxNy), P (0.6CxNy) formed from C12 alkane showed poor solubility and was not appropriate for the complexation of nucleic acids. Notably, P(0.6C8cN6) displayed outperformed protein expression among P(0.6CxN6) group, indicating that appropriate hydrophobicity and structure played a significant role for mRNA transfection, as previously described [29,39,40]. Then, we explored the effect of tertiary amines on mRNA delivery using P(0.6C8cNy) with C8c as the alkane P(0.6C8cN6M) packed with mRNA presented the best transfection efficiency with approximately 85 % GFP^+ cells, which was close to that of Lipo2000 and much higher than that (<10 %) of branched PEI_{25k} (Fig. 1G–S10). Thus, MILP11@mRNA formed from P(0.6C8cN6M) was selected as the optimized formulation for further in vitro and in vivo studies.

The transfection capacity of MILP11@mGFP was assessed in cancer cells. Notably, around 80 % transfection efficiency was achieved in different cancer cells (LLC, U87, SKOV3), in which human U87 and SKOV3 represented around 95 % of GFP^+ cells at a MILP11/mRNA ratio of 20/1 (Fig. 1H). Even at a low MILP11/mRNA mass ratio of 5/1 (N/P ~ 2.5/1), MILP11@mGFP afforded decent transfection efficiencies of 80 % and 60 % in U87 and SKOV-3 cells, respectively (Figs. S11–12). Meanwhile, following long-term storage (5 weeks) at 4 °C, MILP11@mGFP still induced 70 % GFP^+ cells (Figs. 1I) and 75 % MFI of the fresh formulation (Fig. S13A) in 293T cells, in sharp contrast with little transfection of MC3-LNP@mGFP after one-week storage under otherwise the same conditions [41]. In addition, the stability of MILP11@mGFP against lyophilization was evaluated using sucrose as a protectant [41]. When sucrose concentration was greater than 3 % (m/v), the transfection efficiency of lyophilized MILP11@mGFP was comparable to that of fresh one (Fig. 1J and S13B). Besides, the size and zeta potential of lyophilized MILP11@mGFP revealed negligible changes at low sucrose concentrations of 3–6%, while obvious nanoparticle aggregation was observed when the sucrose concentration increased to 12 % (Fig. S14), probably due to that the high viscosity of sucrose interferred with the dispersion of nanoparticles. The retention of mRNA activity and robust physicochemical properties of MILP11@mRNA against long-term storage and lyophilization would greatly facilitate the transportation and clinical application of mRNA drugs.

Interestingly, MILP could proficiently pact pDNA, and the formed MILP@pGFP nanoparticles displayed equivalent transfection efficiency in 293T cells to Lipo2000 complexation (Fig. S15), suggesting that efficient pDNA delivery inside cell nucleus was accomplished by MILP. Thus, MILP emerges as a versatile platform to achieve effective delivery of different nucleic acids including mRNA and DNA in cells. Importantly, different cells (293T, LLC, U87, SKOV) incubated with MILP@mGFP for 24 h all presented over 80 % cell viability (Fig. S16), indicating a decent cytocompatibility.

2.3. MILP-mediated cellular uptake and endosomal escape

Cellular uptake and endosomal escape behaviors were investigated in LLC and 293T cells using Cy5-labeled mRNA (mRNA-Cy5) to further explore the effect of alkanes and tertiary amines on mRNA delivery. In contrast to MILP@mRNA formed from P(0.4CxN6), nanoparticles based on P(0.6CxN6) generally demonstrated significantly higher cellular uptake (Fig. 2A, Fig. S17), corroborating that appropriately increasing hydrophobicity of MILP contributes to the cellular uptake. Among P (0.6CxN6) with C6, C8 and C10 alkanes, the C8 alkane group exhibited more uptake in 293T cells, and cyclic C8c was superior to linear C8 alkanes. One possible explanation is that cyclic alkanes have large steric resistance and mild interactions with lipids in cell membrane, facilitating the membrane crossing of nanoparticles, as previously reported [42]. Then, ionizable lipid-polypeptides with C8c at a mole fraction of 0.6 (P(0.6C8cNy)) were employed to investigate the effect of tertiary amines. The results showed that lipid-polypeptides with 6- and 7-membered cyclic tertiary amines (N6, N6M, N6P and N7) induced superior cellular uptake (Fig. 2A, Fig. S17), possibly owing to the providential balance of hydrophobicity and protonization. Interestingly, the transfection efficacy plotted against cellular uptake efficiency clearly showed that mRNA transfection significantly correlated positively with uptake efficiency ($r = 0.74$ and $P = 0.0002$) (Fig. 2B). The endocytosis pathways were further explored using MILP11@mRNA as an example. The cellular uptake was slightly restrained by methyl--β-cyclodextrin (MβCD) (caveolae), and markedly inhibited by chlorpromazine (clathrin), dynasore (dynamin), and amiloride hydrochloride (macropinocytosis) (Fig. S18), suggesting that clathrin-, dynamin-, and macropinocytosis-mediated internalization pathways were mainly adopted by MILP@mRNA.

The endosomal escape capacity reflected by membrane disruption activity was evaluated by hemolysis assay [43]. At acidic endosomes (pH 5.5), P(0.6CxN6) with more hydrophobic segments exhibited dramatically greater hemolysis than P(0.4CxN6), and P(0.6CxN6) with C6, C8, and C8c alkanes presented hemolysis ratios of 11–17 % (Fig. 2A), supporting their active escape from endosomes. Meanwhile, MILP with different tertiary amines all presented obvious hemolysis, among which MILP from N6, N6M, and N7 revealed a hemolysis ratio of around 15 %. Of note, endosomal escape, reflected by hemolysis ratios, was generally positively correlated with mRNA transfection, as shown in Fig. 2C. Importantly, MILP generally revealed a hemolysis ratio of lower than 5 % at pH 7.4 (Fig. S19), corroborating their hemocompatibility under physiological conditions. The hemolysis switch with pH mainly derived from the protonation of tertiary amines in lipid-polypeptides that had pK_a values of 6.3–7.0 (Fig. S20), and benefited the construction of efficient and safe mRNA delivery systems.

The escape mechanism of MILP11@mRNA in LLC cells was further explored by using a lysosomal disrupting agent (chloroquine, CQ) and a proton pump inhibitor (bafilomycin A1, Baf A1) [44]. The introduction of CQ presented similar GFP expression to MILP11@mRNA alone (Fig. 2D and E), indicating that MILP11-based complexes generated efficient endosomal disruption and escape. Increasing CQ concentration to 100 μM attenuated GFP fluorescence intensity, mainly attributed to the cell death induced by CQ at a high concentration. On the contrary, Baf A1 significantly suppressed the GFP expression in LLC cells, and increasing the Baf A1 concentration induced the declination of fluorsence intensity (Fig. 2D and E), suggesting that the protonation of MILP was a vital prerequisite for the endosomal escape. The protonation degree of lipid-polypeptides under endosomal conditions was reflected by their pK_a values of 6.3–7.0, which might be controlled by selecting different alkanes and tertiary amines and adjusting their ratios. Confocal imaging revealed that most of internalized MILP11@mRNA was initially (2 h incubation) associated with LysoTracker Green DND-26-labeled lysosomes in LLC cells and appeared as yellow dots (Fig. 2F). After 4 h incubation, more yellow dots and red signals appeared, suggesting that more MILP11@mRNA entered lysosomes and some of them even escaped from the lysosomes. After 8 h, yellow dots gradually disappeared and red fluorescence became more scattered. Pearson's correlation coefficient between lysosomes (green) and mLuc-Cy5 (red) quantifying the lysosomal escape decreased with time (Fig. 2G), further supporting the efficient escape of MILP11@mGFP from endosomes [45].

To further understand the interaction between MILP11@mRNA and cell membrane, liposomes were constructed from anionic phosphatidylserine (PS) and used to simulate cell membranes [46]. ITC

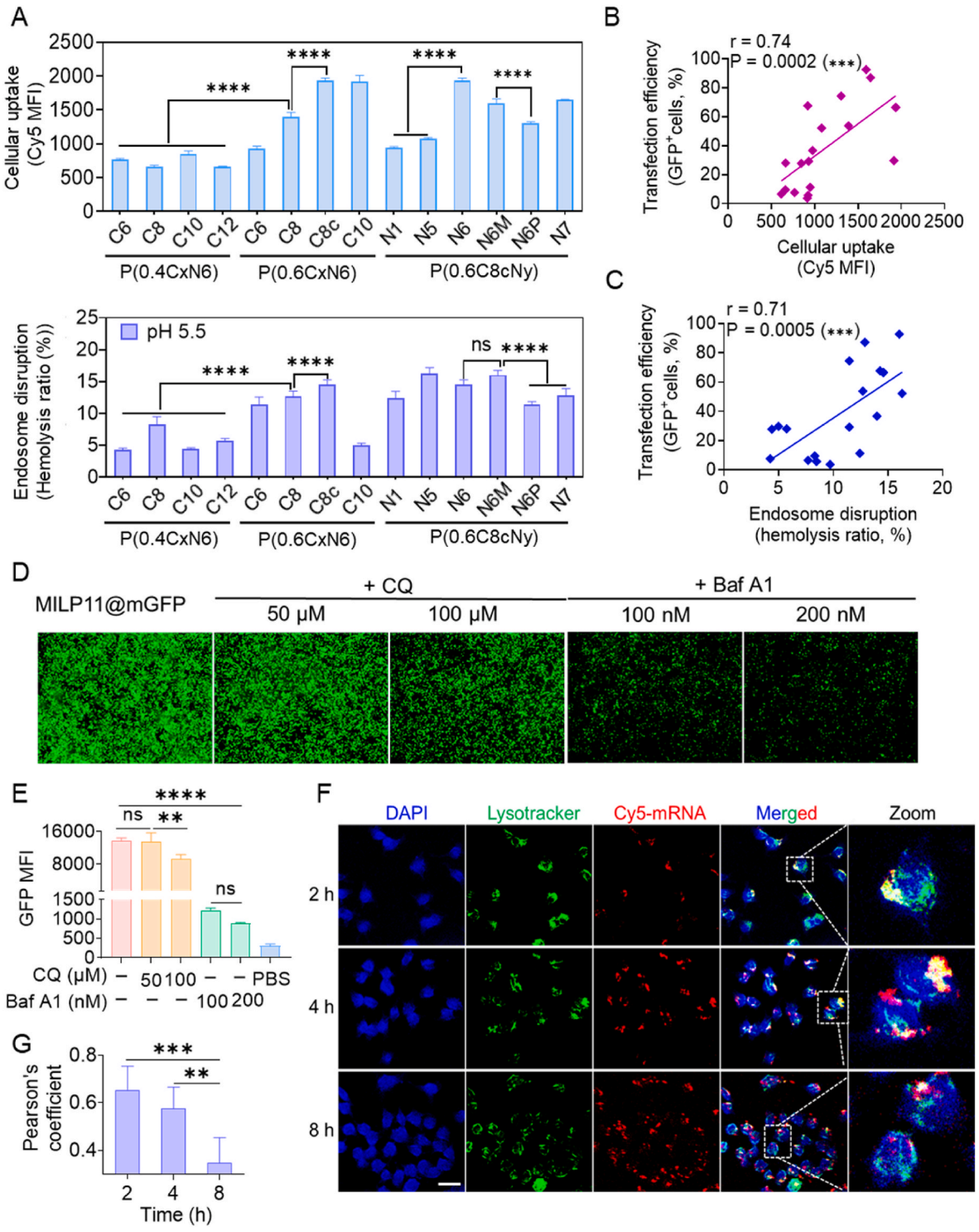

Fig. 2. Comprehensive evaluation of transfection efficiency, cellular uptake, and endosomal disruption of MILP complexed with mRNA in vitro. (A) Cellular uptake and and endosome disruption data (n = 3). Cellular uptake were assessed in 293T cells by flow cytometry. Endosomal disruption was assessed through hemolysis analysis of MILP at pH 5.5. Transfection efficiency of MILP@mGFP was plotted against cellular uptake efficiency (B) and endosomal disruption (C), correlation significance was assessed for MILP@mGFP using Spearman's method, and datasets with statistically significant correlations were indicated with fitted lines. (D–E) Endosomal escape of MILP11@mGFP. Effect of chloroquine (CQ) (D) and bafilomycin A1 (Baf A1) (E) on the transfection of MILP11@mGFP in Lewis lung carcinoma (LLC) cells following 24 h incubation (mGFP: 1.0 μg/mL, n = 3). (F) Confocal images of LLC cells incubated with MILP11@mLuc-Cy5 for 2, 4, or 8 h (mLuc: 1.0 μg/mL); mLuc labeled with Cy5 is shown in red, the cell nuclei stained with DAPI are shown in blue, and lysosomes stained with LysoTracker Green DND-26 are shown in green. Scale bar: 20 μm. (G) Pearson's correlation coefficient (Pearson's R value) between lysosomes (green) and mLuc-Cy5 (red) quantifying the lysosomal escape (n = 5). Statistical significance in (E, G) was analyzed by one-way ANOVA with Tukey's multiple comparisons test. (ns, not significant; $^{*}p < 0.05$, $^{**}p < 0.01$, $^{***}p < 0.001$, $^{****}p < 0.0001$).

measurement showed that the binding capacity of P(0.6C8cN6M) to liposomes was significantly high with binding constants of 1.2×10^8 M^{-1} (Ka1) and 8.2×10^7 M^{-1} (Ka2) (Fig. S21 and Table S3), while P(N6M) presented two to three orders lower binding constants, suggesting that MILP11@mRNA minght form multivalent interactions with cell and endosome membrane to facilitate the cellular uptake and endosomal escape, respectively.

2.4. Tumor-confined biodistribution and expression of MILP@mRNA

The in vivo biodistribution and protein expression of MILP11@mLuc were investigated in LLC tumor-bearing mice. LNP@mLuc formed from ionizable SM-102 lipid which had an average diameter of approximate 100 nm and neutral surface charge was used as a control (Fig. S22). In vivo bioluminescence imaging showed that after intratumoral injection, MILP11@mLuc promoted tumor-confined luciferase expression within LLC (Fig. 3A and B) and 4T1 (Fig. S23) tumors in sharp contrast with scattered distribution of luciferase fluorescence within both tumor and abdomen in LNP@mLuc group. The tumor-confined protein expression of MILP11@mLuc was also clearly observed by ex vivo fluorescence imaging (Fig. 3C). Meanwhile, the biodistribution was monitored using mLuc labeled with Cy5 (mLuc-Cy5). Consistent with the protein expression, intratumoral administration of MILP11@mLuc for 6 h induced mRNA distribution only within tumors, while strong Cy5

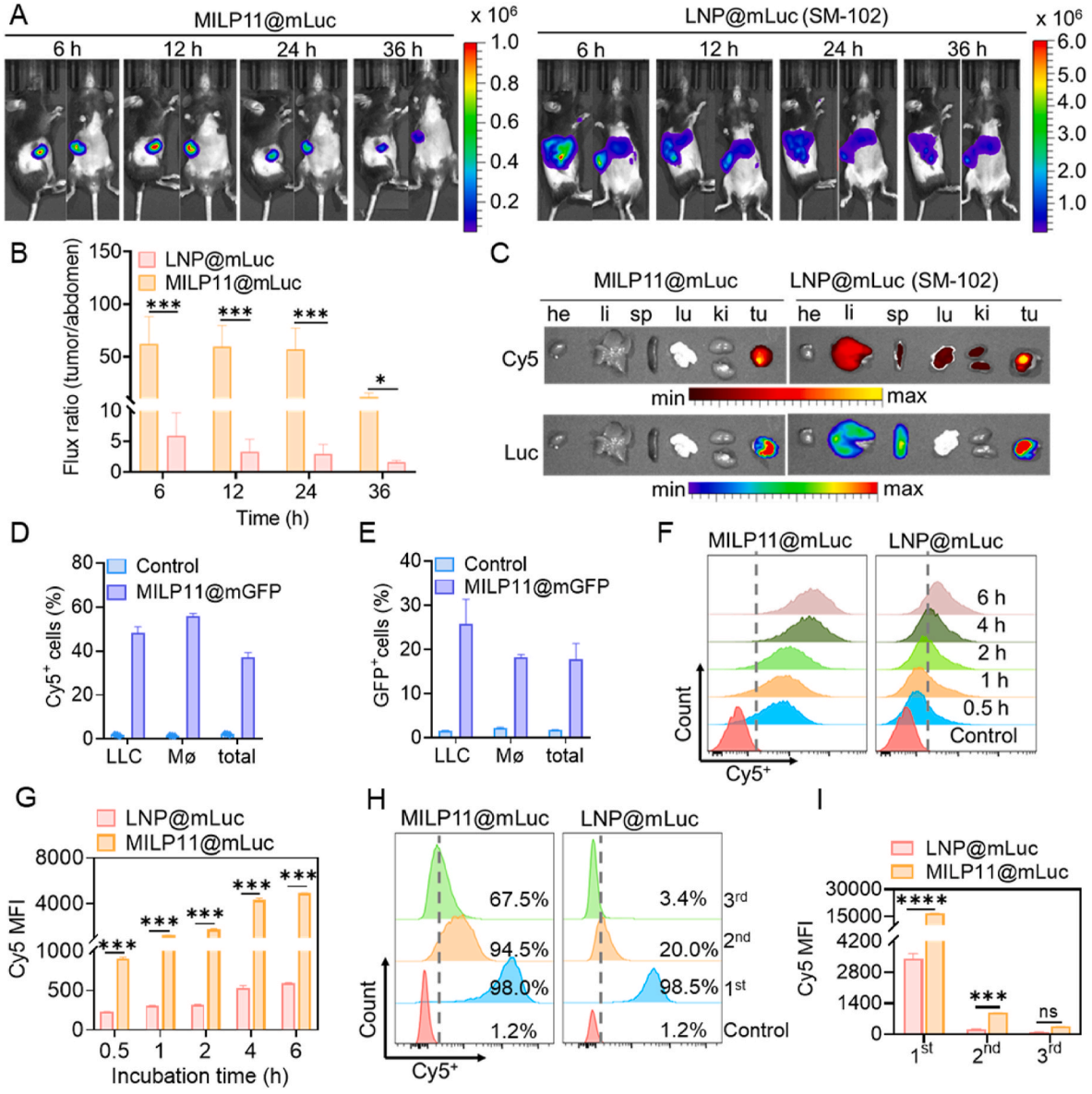

Fig. 3. Biodistribution and mRNA expression after intratumoral injection in subcutaneous LLC model. (A) Bioluminescence imaging of injected mice taken at different time points using the IVIS imaging system (n = 3). (B) Photon flux ratios of the tumors to the abdomen. LNP@mLuc from SM-102 was used as a control. (C) Ex vivo images showing biodistribution (Cy5) and luciferase expression (Luc) of MILP11@mLuc and LNP@mLuc in tumors and major organs at 6 h after injection (mLuc-Cy5: 0.5 mg/kg). (D–E) Representative flow cytometry analysis of cellular uptake (D) and mGFP expression (E) in different cells (LLC cells, $CD45^-$ $CD44^+$; macrophages (Mφ), $CD45^+$ $F4/80^+$) of LLC tumors (n = 3). After intratumoral injection of MILP11@mGFP for 12 h, the tumors were dissected and analyzed by flow cytometry (mGFP: 0.5 mg/kg). (F–G) Cellular uptake of MILP11@mLuc and LNP@mLuc in LLC cells at different time points. (mLuc-Cy5: 1.0 μg/mL, n = 3). Percentages of $Cy5^+$ LLC cells (F) and Mean fluorescence intensity (MFI) (G) of Cy5 positive cells measured using flow cytometry. (H–I) Intercellular trafficking of MILP11@mLuc-Cy5 and LNP@mLuc-Cy5 among LLC cells (n = 3). Percentages of $Cy5^+$ LLC cells (H) and MFI (I) of Cy5 positive cells in different batches were analyzed via flow cytometry. Statistical significance in (B, G and I) was analyzed by one-way ANOVA with Tukey's multiple comparisons test. (ns, not significant; *$p < 0.05$, **$p < 0.01$, ***$p < 0.001$, ****$p < 0.0001$).

fluorescence was detected in the tumors and major organs (liver, lung, kindy, and spleen) in LNP@mLuc group (Fig. 3C). As previously described, LNP generated from SM-102 or ALC0315 showed scattered mRNA distribution and protein expression in major organs after intramuscular and intratumoral injection [47]. Notably, Notably, PEI_{25k}@mLuc although showing apparent protein expression at tumor sites after intratumoral administration presented much less bioluminescence flux comparing with MILP@mLuc (Fig. S24). Following intramuscular and subcutaneous injection, MILP11@mLuc although dominantly residing at the injection sites displayed little protein expression (Fig. S25), verifying the low transfection efficiency of MILP11@mRNA in skin and muscle tissues. Besides, histological analysis revealed that MILP11@mLuc induced no cell apoptosis and necrosis of adjacent skin tissue (Fig. S26).

The biodistribution and transfection of MILP11@mRNA were further assessed in LLC cells and tumor-associated macrophages (TAMs, Mφ) considering that they account for a dominant portion (around 90 %) of the tumors. Notably, about 48.5 % of LLC cells ($CD45^{-}CD44^{+}$), 55.7 % of the TAMs ($CD45^{+}F4/80^{+}$), and 37.0 % of the total cells isolated from the tumor were Cy5 positive (Fig. 3D, Fig. S27A), corroborating the extensive distribution and efficient cellular uptake of MILP11@mRNA in the tumors. Correspondingly, significant GFP expression was observed in LLC cells (25.7 %) and TAMs (18.2 %), while total cells presented less GFP^{+} cells (17.8 %) as a result from the lower transfection of MILP@mRNA in other cells (Fig. 3E, Fig. S27B).

The trafficking of nanoparticles in the tumor microenvironment (TME) is mainly driven by diffusion, convection or cell-based mechanisms, and thus depends on the interactions with tumor cells and intercellular components [48]. The interaction of nanoparticles with tumor cells was explored, and the results revealed that more than 90 % of LLC cells took up MILP11@mLuc-Cy5 while LNP@mLuc-Cy5 (SM-102) group induced about 30 % $Cy5^{+}$ LLC cells after 0.5 h incubation (Fig. 3F–G). When the incubation time was extended to 6 h, the uptake of MILP11@mEGFP-Cy5 was 8-fold higher than that of LNP@mLuc-Cy5, primarily attributing to the multivalent interactions of MILP with the cell membrane (Fig. 3F–G). Besides, MILP11@mRNA with multivalent interaction sites could provide strong affinity with extracellular matrix mainly composing of collagen and hyaluronic acid, facilitating the localization of the nanoparticles in TME, similar to polyethylenimine modified porous silica nanoparticles [32].

The intercellular delivery behavior of MILP11@mLuc was investigated to explore the transportation among cells in tumor and LNP@mLuc as control. LLC cells were first treated with MILP11@mLuc for 6 h and then cultured in a fresh medium for another 12 h. The cells were denoted as the 1st batch, and the culture medium 1 was collected and employed for the culture of fresh LLC cells. After 12 h incubation, the cells were denoted as the 2nd batch, and then cultured with a fresh medium for another 12 h to obtain the medium 2 containing released complexes. Following the culture of fresh LLC cells with the medium 2 for 12 h incubation, the cultured cells were denoted as the 3rd batch (Fig. S28). Although the percentage of $Cy5^{+}$ LLC cells decreased from over 98.0 %–67.5 % from the 1st batch to the 3rd batch, the majority of the cells in the 3rd batch contained nanoparticles as characterized by flow cytometry (Fig. 3H–I), indicating that internalized MILP11@mLuc could released into the medium and enter adjacent cancer cells. On the contrary, LNP afforded much less $Cy5^{+}$ cells with 20 % and 3.4 % in 2nd and 3rd batches (Fig. 3H–I). Notably, remarkably gradual decrease of Cy5 MFI was observed from the 1st batch to 3rd batch, signifying the partial retention of MILP11@mRNA in tumor cells in the process of transcytosis (Fig. 3I). On the contrary, LNP afforded inferior transcytosis with much less $Cy5^{+}$ cells in the 2nd (20 %) and 3rd (3.4 %) batches (Fig. 3H–I). The intercellular trafficking behavior of MILP11@mRNA in tumors might be closely associated with the multivalent interaction-dependent cellular uptake and the robust stability upon crossing cells.

2.5. In vivo antitumor activity of MILP@mIL-12

Encouraged by the exclusive distribution and efficient protein expression at tumor sites, we further explored the tumor-confined transfection and antitumor potential of therapeutic mRNA delivered by MILP11. 4T1 and LLC tumor models were used in this study considering that MILP11@mRNA revealed high transfection efficiency in the cancer cells, and breast and lung lesions can now be readily accessed without or with the assistance of imaging modalities. Interleukin 12 (IL-12) is a potent proinflammatory cytokine that promotes T-cell proliferation and activation and is effective in stimulating interferon-γ (IFN-γ) production, and therefore is considered to be a promising anticancer agent [49]. Unfortunately, the clinical application of IL-12 is limited by the short half-life, insufficient local concentration within tumors, and immune-related adverse events. Here, MILP11 encapsulated with mRNA encoding IL-12 (MILP11@mIL-12) was employed to ameliorate immunosuppressive tumor environment. Notably, MILP11@mIL-12 induced significant IL-12 expression in LLC cells in vitro (Fig. 4A), and tumor-confined IL-12 enrichment with over 9-fold higher protein expression in the tumor than that in the liver at 6–12 h post-administration (Fig. 4B). On the contrary, LNP@mIL-12 generated comparable IL-12 levels in the tumor to those in the liver under otherwise the same conditions (Fig. 4B). Importantly, MILP11@mIL-12 generated much less IL-12 in the blood than LNP@mIL-12 (250 vs 1500 pg/mL) (Fig. 4C), suggesting that MILP11@mIL-12 unlikely induced the systemic immunotoxicity. Meanwhile, mice treated with MILP11@mIL-12 presented little body weight change (Fig. S29), normal hepatorenal function and histological structure (Fig. S30, Table S4), supporting the outstanding safety of MILP11@mIL-12 formulation. In mice-bearing LLC tumor xenografts, MILP11@mIL-12 offered significant suppression of tumor growth and largely extended survival time, while free mIL-12 showed a little effect on tumor inhibition and mouse survival (Fig. 4E–G), signifying the vital role of MILP11 delivery system. Besides, non-therapeutic MILP11@mLuc induced minimal suppression on tumor growth (Fig. 4E–G), affording a negligible therapeutic effect. In combination with αPD-1, MILP11@mIL-12+αPD-1 group resulted in better growth inhibition of LLC tumors and a remarkably high survival rate with 50 % mouse survival during the experimental period, while no mice was survived and a median survival time (MST) of 25 days were presented in MILP11@mIL-12 only group (Fig. 4G). Similarly, MILP11@mIL-12+αPD-1 group demonstrated more prominent tumor suppression and survival extension in 4T1 tumor-bearing mice than MILP11@mIL-12 group (MST 33 vs29) (Fig. S31). Therefore, intratumoral administration MILP11@mRNA with superior efficacy and minimum off-target toxicity hold significant potential on the treatment of various malignant tumors like breast, melanoma, and lung cancers. However, imaging or surgical assistance might be required for performing intratumoral injection in many tumors, which would compromise the clinical applications.

2.6. MILP@mIL-12-mediated modulation of tumor microenvironments

IL-12 is known to stimulate the proliferation of $CD8^{+}$ T cells and thus affords an increase of cytotoxic activity towards tumors [50]. Besides, IL-12 can also promote IFN-γ production, activate dendritic cells, and remodulate the immunosuppressive TME (Fig. 5A). Following three-dose treatment, as shown in Fig. 4D, the tumors and their adjacent tumor-draining lymph nodes (TDLNs) were harvested at day 9 for immunoassay using flow cytometry (Figs. S32–33). Both MILP11@mIL-12 and MILP11@mIL-12+αPD-1 evidently increased the infiltration of $CD45^{+}$ immune cells (Fig. 5B) and $CD8^{+}$ T cells (Fig. 5C and D), as well as the populations of activated $CD8^{+}$ T cells ($CD8^{+}$ $CD25^{+}$ T) (Fig. 5E) and IFN-γ^{+} $CD8^{+}$ T cells (Fig. 5F). Meanwhile, the populations of the immunosuppressive cells including Tregs ($CD4^{+}$ $FOXP3^{+}$) and MDSCs ($CD11b^{+}$ $Gr\text{-}1^{+}$) in the tumors significantly declined following the treatment with MILP11@mIL-12 or

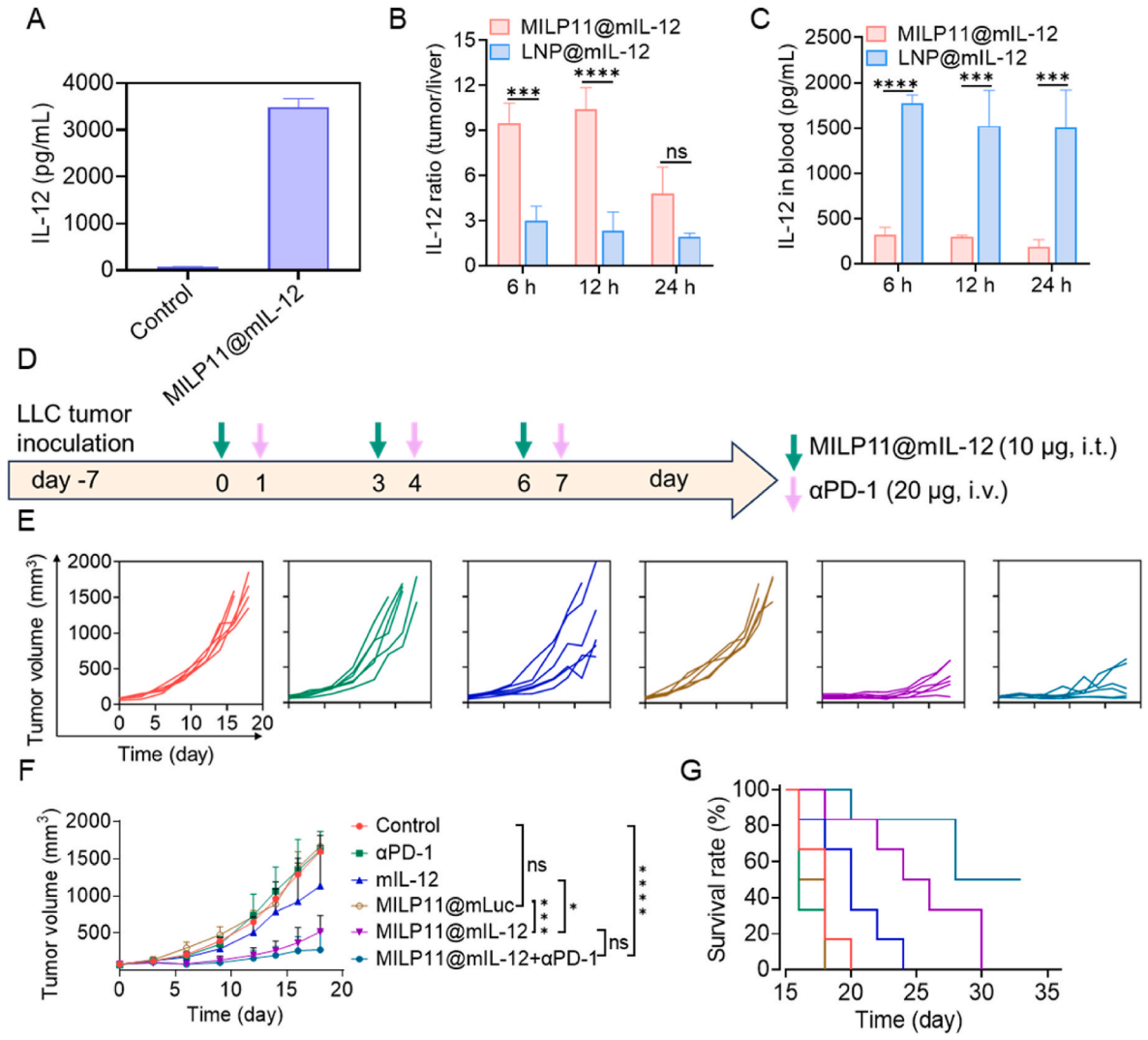

Fig. 4. MILP11@mIL-12 elicits strong antitumor effect in subcutaneous LLC tumor xenografts. (A) IL-12 secretion in LLC cells transfected with MILP11@mIL-12 for 24 h (n = 3). (B) Ratios of IL-12 in tumor to that in liver, and (C) IL-12 expression in peripheral blood after intratumoral injection of MILP11@mIL-12 and LNP@mIL-12 in LLC tumor-bearing mice. Data are presented as mean ± SD, n = 3. (D) Schematic of MILP11@mIL-12 and αPD-1 dosing regimen. When the tumor volume reached about 100 mm^3, MILP11@mIL-12 and MILP11@mLuc was injected intratumorally (10 μg/mouse/dose), and αPD-1 (20 μg/mice/dose) was administered via the tail vein in the following day. (E–F) Individual and average tumor volume curves over time (n = 6). (G) Kaplan-Meier survival plots for mice bearing LLC tumors over time (n = 6). Statistical analysis in (B, C and F)was performed by one-way ANOVA with Tukey's multiple comparisons test. Survival rate in G was analyzed by Kaplan-Meier technique with a log-rank (Mantel-Cox) test. (ns, not significant; $^*p < 0.05$, $^{**}p < 0.01$, $^{***}p < 0.001$, $^{****}p < 0.0001$).

MILP11@mIL-12+αPD-1 (Fig. 5G and H). Comparing with free mIL-12, MILP11@mIL-12 impelled the polarization of macrophages towards M1 phenotype and presented a significantly lower M2/M1 ratio (Fig. 5I). In the TDLNs, significant increase of $CD80^+$ DC and slight elevation of $MHCII^+$ DC were detected in both MILP11@mIL-12 and MILP11@mIL-12+PD-1 groups (Fig. 5J and K).These results indicate that MILP11@mIL-12 combined with α-PD-1 can enhance the infiltration of antitumor immune cells and ameliorate the immunosuppressive TME.

3. Discussion

Advances in mRNA-based therapies are emerging to revolutionize the treatment of various diseases including cancers, considering that mRNA can be translated into functional proteins that either directly inhibit tumor progression or trigger and strengthen immune responses [3,51]. With the help of LNP, more than 1000 clinical trials of mRNA-based therapies have been conducted. However, the LNP systems still confront several challenges, such as nonselective delivery, potential adverse effects derived from PEG and cationic lipids, complex components based on four lipids, and unsatisfactory stability, which requires ultralow temperature for transportation and storage [12].

Here, a library of multivalent ionizable lipid-polypeptides (MILP) based on polyaspartamide derivatives have been explored to achieve robust mRNA complexation and tumor-confined transfection. Considering that electrostatic and hydrophobic interactions play imperative roles for the complexation and delivery of nucleic acids [28], different tertiary amines and alkanes with varying ratios were employed and optimized to adjust the hydrophobicity, pK_a, and functionalities of the lipid-polypeptides. Among the 13 candidates, P(0.6C8cN6M) denoted as MILP11 was identified as the top-performing lipid-polypeptide, which efficiently packed both mRNA and DNA, and afforded comparable in vitro transfection efficiency to the commercial Lipo2000, suggesting that MILP enabled effective delivery of nucleic acids to cytoplasma and cell nucleus. It is not usual to achieve efficient delivery of both mRNA and DNA with the same vehicle since the two nucleic acids have quite different sizes and structure [52]. In contrast with LNP that prepared with four lipids, MILP@mRNA/DNA was constructed with one ingredient via simple vortex, facilitating the preparation and scale-up of

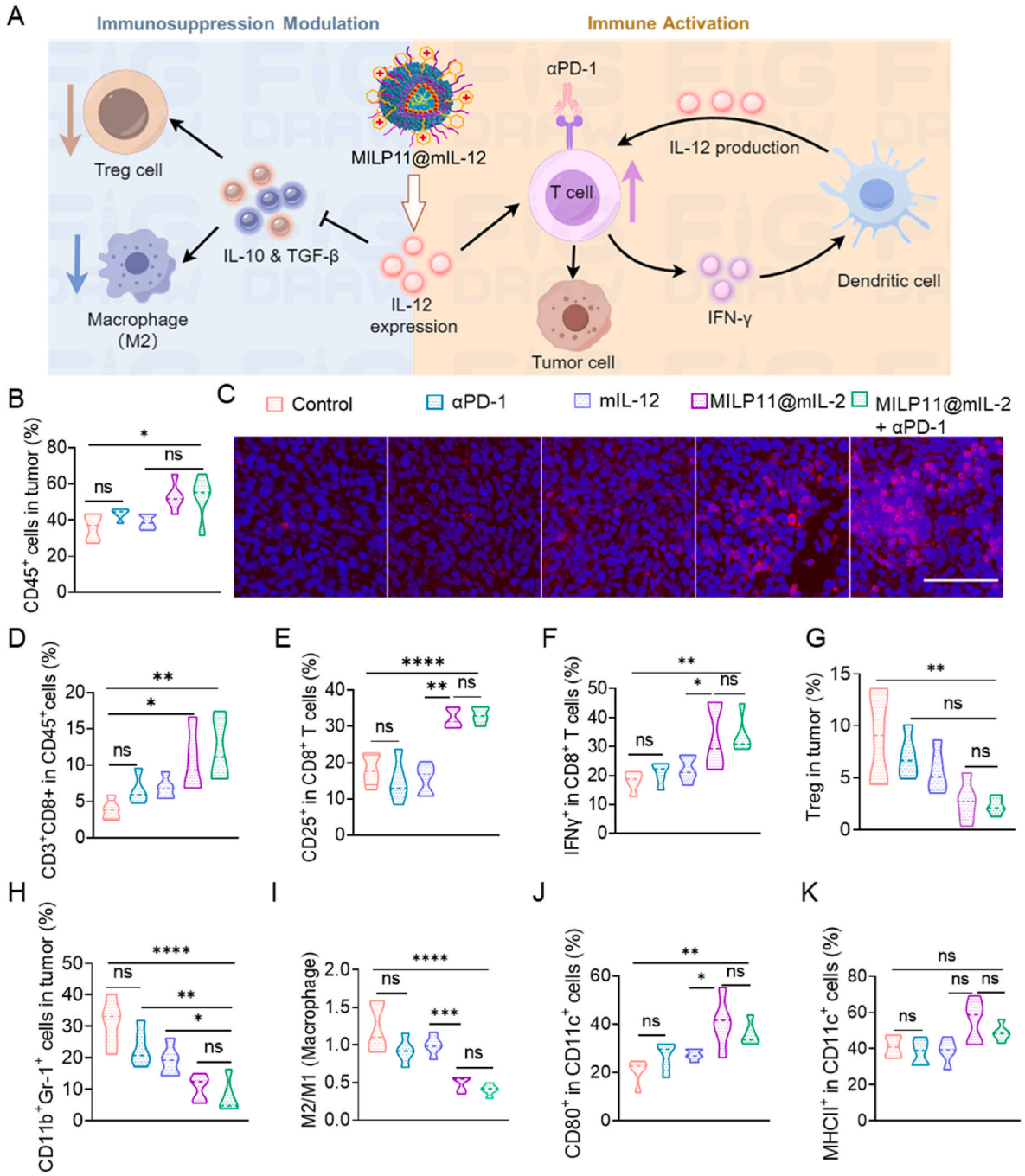

Fig. 5. MILP11@mIL-12 modulates the TME in LLC xenografts. The formulations were administered as shown in Fig. 4D, and the tumors dissected two days after the last treatment were digested to isolate all the cells for flow cytometry analysis. (A) Illustration of the mechanism by which MILP11@mIL-12 modulates the TME (n = 5). (B) Percentage of $CD45^+$ cells among the live cells of the tumors. (C) Immunostaining of the $CD8^+$ T (red) in the tumor sections. Scale bar: 50 μm. (D) Percentage of $CD8^+$ T cells among the $CD45^+$ cells. (E) Percentage of activated T cells ($CD25^+$) among the $CD8^+$ T cells. (F) Percentage of IFN-γ^+ cells among the $CD8^+$ T cells. (G) Percentage of Tregs ($FOXP3^+$) among $CD4^+$ T cells. (H) Percentage of MDSCs ($CD11b^+$ $Gr\text{-}1^+$) among live cells. (I) Ratios of M2/M1 macrophages. (J) Percentage of $CD80^+$ cells among DCs in the TDLNs. (K) Percentage of $MHCII^+$ cells among DCs in the TDLNs. Statistical analysis was performed by one-way ANOVA with Tukey's multiple comparisons test. (ns, not significant; *$p < 0.05$, **$p < 0.01$, ***$p < 0.001$, ****$p < 0.0001$).

nucleic acid drugs. By mimicking multivalent electrostatic, hydrophobic, and H-bond interactions in many biochemical processes, MILP@mRNA demonstrates high encapsulation efficiency (>90 %), monodisperse small sizes, and remarkable stability against lyophilization and long-term storage (~5 weeks). On the contrary, mRNA-1273 and BNT162b2 are required to store at −15 ~ −20 °C and −60 ~ −80 °C, respectively, followed by thawing for administration.

Specific and efficient delivery of mRNA to target lesions would greatly benefit the treatment of a variety of diseases. LNP@mRNA tends to accumulate in the liver following administration, which often compromises the therapeutic outcomes and induces liver injury [13]. In mice bearing subcutaneous LLC tumors, MILP@mRNA induces exclusive tumor residence and distribution via multivalency-directed strong affinity and transcytosis, and affords specific protein expression in tumor cells and macrophages at tumor sites following intratumoral injection, in sharp contrast to the indiscriminate distribution and transfection in main organs of SM-102 LNP. The tumor-confined distribution and protein expression would not only maximize the therapeutic efficacy, but

also minimize the possible off-target adverse effects from both mRNA and vehicles. Although several LNP systems were reported to attain selective mRNA expression in targeted organs, most of them displayed dominant distribution in liver tissue [53,54]. The tumor-confined distribution of MILP@mRNA might be attributed to multivalency-directed strong interactions with cell membrane and extracellular matrix enriching with negatively charged proteins and polysaccharides, affording accelerated cellular uptake, facile intercellular trafficking via transcytosis, and robust retention at tumor sites [55].

Cytokines as vital mediators of cell communication can provide direct anti-proliferative activity towards tumor cells or indirect cytotoxic activity by stimulating immune cells [56]. Although two cytokines (interferon-α and IL-2) have been approved for the treatment of hairy cell leukemia, advanced renal cell carcinoma, and metastatic melanoma, they often display mild clinical benefits mainly owing to the short half-lives and severe systemic adverse toxicity [50]. Here, MILP11@mIL-12 induced over 9-fold higher protein expression in the tumor than that in the liver, in sharp contrast to comparable IL-12 levels in the tumor to those in the liver provided by SM-102 LNP formulation under otherwise the same conditions. Importantly, MILP11@mIL-12 generated much less IL-12 in the blood than LNP@mIL-12 (250 vs 1500 pg/mL), and caused little change of body weights, hepatorenal function and histological structure, suggesting that MILP@mIL-12 unlikely induced the systemic immunotoxicity. Meanwhile, MILP@mIL-12 significantly remodeled the tumor immunoenvironment by eliciting infiltration and activation of effector T cells and DC, secretion of IFN-γ, and inhibiting the presence of immunosuppressive cells (Tregs, MDSCs), resulting in remarkable therapeutic potential towards subcutaneous LLC and 4T1 tumor xenografts. Cytokines in combination with immune checkpoint therapy has been reported to generate synergistic anticancer mechanisms and maximize therapeutic efficacy [57]. In mice bearing subcutaneous tumor xenografts, MILP@mIL-12 combined with αPD-1 afforded the greatest inhibition of tumor growth and significantly prolonged survival time.

4. Conclusion

We have demonstrated that multivalent ionizable lipid-polypeptides (MILP) can be readily developed and employed for robust mRNA complexation and tumor-confined transfection. By mimicking multivalent electrostatic, hydrophobic, and H-bond interactions in numerous biochemical processes, MILP afforded robust affinity for the complexation of nucleic acids (mRNA, DNA), cell binding, and endosomal disruption. MILP complexed with mRNA (MILP@mRNA) revealed high stability against long-term storage and lyophilization, 8-fold more cellular uptake than SM-102 LNP, high transfection in different cells, and tumor-confined distribution and specific protein expression following intratumoral injection. In subcutaneous LLC and 4T1 tumor xenografts, MILP@mIL-12 elicited exclusive IL-12 expression at tumor sites, and afforded significant remodeling of the tumor immunoenvironments and remarkable antitumor activity with significantly prolonged survival time. Thus, MILP offering biomimetic multivalent interactions for robust complexation, site-specific delivery, and efficient transfection of mRNA would potentially expand the applications of nucleic acid drugs.

CRediT authorship contribution statement

Xiaofei Zhao: Writing – original draft, Validation, Methodology, Investigation, Formal analysis, Data curation. **Yueyue Zhang:** Methodology, Investigation. **Xin Wang:** Methodology, Investigation. **Ziming Fu:** Methodology, Investigation. **Zhiyuan Zhong:** Writing – review & editing, Project administration, Formal analysis, Conceptualization. **Chao Deng:** Writing – review & editing, Supervision, Project administration, Funding acquisition, Conceptualization.

Ethics approval and consent to participate

All animal experiments were approved by the Animal Care and Use Committee of Soochow University (P.R. China), and all protocols conformed to the Guide for the Care and Use of Laboratory Animals.

Declaration of competing interest

The authors declare that they have no known competing financial interests or personal relationships that could have appeared to influence the work reported in this paper.

Acknowledgments

The financial support from the National Key R&D Program of China (2021YFB3800900, 2022YFB3804600), and the National Natural Science Foundation of China (NSFC 52373299) is acknowledged.

Appendix A. Supplementary data

Supplementary data to this article can be found online at https://doi.org/10.1016/j.bioactmat.2024.12.032.

References

[1] X. Hou, T. Zaks, R. Langer, Y. Dong, Lipid nanoparticles for mRNA delivery, Nat. Rev. Mater. 6 (2021) 1078–1094, https://doi.org/10.1038/s41578-021-00358-0.
[2] A.J. Barbier, A.Y. Jiang, P. Zhang, R. Wooster, D.G. Anderson, The clinical progress of mRNA vaccines and immunotherapies, Nat. Biotechnol. 40 (2022) 840–854, https://doi.org/10.1038/s41587-022-01294-2.
[3] X. Huang, N. Kong, X. Zhang, Y. Cao, R. Langer, W. Tao, The landscape of mRNA nanomedicine, Nat. Med. 28 (2022) 2273–2287, https://doi.org/10.1038/s41591-022-02061-1.
[4] E. Rohner, R. Yang, K.S. Foo, A. Goedel, K.R. Chien, Unlocking the promise of mRNA therapeutics, Nat. Biotechnol. 40 (2022) 1586–1600, https://doi.org/10.1038/s41587-022-01491-z.
[5] Y. Xiao, Z. Tang, X. Huang, W. Chen, J. Zhou, H. Liu, C. Liu, N. Kong, W. Tao, Emerging mRNA technologies: delivery strategies and biomedical applications, Chem. Soc. Rev. 51 (2022) 3828–3845, https://doi.org/10.1039/d1cs00617g.
[6] Y. Zhang, Y. Hu, H. Tian, X. Chen, Opportunities and challenges for mRNA delivery nanoplatforms, J. Phys. Chem. Lett. 13 (2022) 1314–1322, https://doi.org/10.1021/acs.jpclett.1c03898.
[7] P. Huang, H. Deng, C. Wang, Y. Zhou, X. Chen, Cellular trafficking of nanotechnology-mediated mRNA delivery, Adv. Mater. 36 (2024) e2307822, https://doi.org/10.1002/adma.202307822.
[8] S. Qin, X. Tang, Y. Chen, K. Chen, N. Fan, W. Xiao, Q. Zheng, G. Li, Y. Teng, M. Wu, X. Song, mRNA-based therapeutics: powerful and versatile tools to combat diseases, Signal Transduct. Targeted Ther. 7 (2022) 166, https://doi.org/10.1038/s41392-022-01007-w.
[9] S. Douka, L.E. Brandenburg, C. Casadidio, J. Walther, B.B.M. Garcia, J. Spanholtz, M. Raimo, W.E. Hennink, E. Mastrobattista, M. Caiazzo, Lipid nanoparticle-mediated messenger RNA delivery for ex vivo engineering of natural killer cells, J. Contr. Release 361 (2023) 455–469, https://doi.org/10.1016/j.jconrel.2023.08.014.
[10] S.A. Lim, A. Cox, M. Tung, E.J. Chung, Clinical progress of nanomedicine-based RNA therapies, Bioact. Mater. 12 (2022) 203–213, https://doi.org/10.1016/j.bioactmat.2021.10.018.
[11] D. Loughrey, J.E. Dahlman, Non-liver mRNA delivery, Acc. Chem. Res. 55 (2022) 13–23, https://doi.org/10.1021/acs.accounts.1c00601.
[12] D. Bitounis, E. Jacquinet, M.A. Rogers, M.M. Amiji, Strategies to reduce the risks of mRNA drug and vaccine toxicity, Nat. Rev. Drug Discov. 23 (2024) 281–300, https://doi.org/10.1038/s41573-023-00859-3.
[13] M. Alden, F. Olofsson Falla, D. Yang, M. Barghouth, C. Luan, M. Rasmussen, Y. De Marinis, Intracellular reverse transcription of pfizer BioNTech COVID-19 mRNA vaccine BNT162b2 in vitro in human liver cell line, Curr. Issues Mol. Biol. 44 (2022) 1115–1126, https://doi.org/10.3390/cimb44030073.
[14] S.-H. Bae, S. Yoo, J. Lee, H.-J. Park, S.P. Kwon, H. Jin, S.-I. Park, Y.-S. Lee, Y.-J. Bang, G. Roh, S. Lee, S.B. Youn, I.W. Kim, H.R. Oh, A.K. El-Damasy, G. Keum, H. Kim, H. Youn, J.-H. Nam, E.-K. Bang, A lipid nanoparticle platform incorporating trehalose glycolipid for exceptional mRNA vaccine safety, Bioact. Mater. 38 (2024) 486–498, https://doi.org/10.1016/j.bioactmat.2024.05.012.
[15] J. Chen, Z. Ye, C. Huang, M. Qiu, D. Song, Y. Li, Q. Xu, Lipid nanoparticle-mediated lymph node-targeting delivery of mRNA cancer vaccine elicits robust CD8(+) T cell response, Proc. Natl. Acad. Sci. USA 119 (2022) e2207841119, https://doi.org/10.1073/pnas.2207841119.
[16] M. Qiu, Y. Tang, J. Chen, R. Muriph, Z. Ye, C. Huang, J. Evans, E.P. Henske, Q. Xu, Lung-selective mRNA delivery of synthetic lipid nanoparticles for the treatment of

pulmonary lymphangioleiomyomatosis, Proc. Natl. Acad. Sci. USA 119 (2022) e2116271119, https://doi.org/10.1073/pnas.2116271119.
[17] Z. He, Z. Le, Y. Shi, L. Liu, Z. Liu, Y. Chen, A multidimensional approach to modulating ionizable lipids for high-performing and organ-selective mRNA delivery, Angew. Chem. Int. Ed. 62 (2023) e202310401, https://doi.org/10.1002/anie.202310401.
[18] X. Zhang, K. Su, S. Wu, L. Lin, S. He, X. Yan, L. Shi, S. Liu, One-component cationic lipids for systemic mRNA delivery to splenic T cells, Angew. Chem. Int. Ed. 63 (2024) e202405444, https://doi.org/10.1002/anie.202405444.
[19] Q. Cheng, T. Wei, L. Farbiak, L.T. Johnson, S.A. Dilliard, D.J. Siegwart, Selective organ targeting (SORT) nanoparticles for tissue-specific mRNA delivery and CRISPR–Cas gene editing, Nat. Nanotechnol. 15 (2020) 313–320, https://doi.org/10.1038/s41565-020-0669-6.
[20] S.A. Dilliard, Q. Cheng, D.J. Siegwart, On the mechanism of tissue-specific mRNA delivery by selective organ targeting nanoparticles, Proc. Natl. Acad. Sci. USA 118 (2021) e2109256118, https://doi.org/10.1073/pnas.2109256118.
[21] E. Álvarez-Benedicto, Z. Tian, S. Chatterjee, D. Orlando, M. Kim, E.D. Guerrero, X. Wang, D.J. Siegwart, Spleen SORT LNP generated in situ CAR T cells extend survival in a mouse model of lymphoreplete B cell lymphoma, Angew. Chem. Int. Ed. 62 (2023) e202310395, https://doi.org/10.1002/anie.202310395.
[22] J.G. Rurik, I. Tombacz, A. Yadegari, P.O.M. Fernandez, S.V. Shewale, L. Li, T. Kimura, O.Y. Soliman, T.E. Papp, Y.K. Tam, B.L. Mui, S.M. Albelda, E. Pure, C. H. June, H. Aghajanian, D. Weissman, H. Parhiz, J.A. Epstein, CAR T cells produced in vivo to treat cardiac injury, Science 375 (2022) 91–96, https://doi.org/10.1126/science.abm0594.
[23] L. Xue, N. Gong, S.J. Shepherd, X. Xiong, X. Liao, X. Han, G. Zhao, C. Song, X. Huang, H. Zhang, M.S. Padilla, J. Qin, Y. Shi, M.G. Alameh, D.J. Pochan, K. Wang, F. Long, D. Weissman, M.J. Mitchell, Rational design of bisphosphonate lipid-like materials for mRNA delivery to the bone microenvironment, J. Am. Chem. Soc. 144 (2022) 9926–9937, https://doi.org/10.1021/jacs.2c02706.
[24] Y. Hagino, I.A. Khalil, S. Kimura, K. Kusumoto, H. Harashima, GALA-modified lipid nanoparticles for the targeted delivery of plasmid DNA to the lungs, Mol. Pharm. 18 (2021) 878–888, https://doi.org/10.1021/acs.molpharmaceut.0c00854.
[25] J.C. Kaczmarek, A.K. Patel, K.J. Kauffman, O.S. Fenton, M.J. Webber, M. W. Heartlein, F. DeRosa, D.G. Anderson, Polymer–LipidNanoparticlesfor systemic delivery of mRNAtothe lungs, Angew. Chem. Int. Ed. 55 (2016) 13808–13812, https://doi.org/10.1002/anie.201608450.
[26] J.C. Kaczmarek, A.K. Patel, L.H. Rhym, U.C. Palmiero, B. Bhat, M.W. Heartlein, F. DeRosa, D.G. Anderson, Systemic delivery of mRNA and DNA to the lung using polymer-lipid nanoparticles, Biomaterials 275 (2021) 120966, https://doi.org/10.1016/j.biomaterials.2021.120966.
[27] Z. Li, L. Amaya, A. Ee, S.K. Wang, A. Ranjan, R.M. Waymouth, H.Y. Chang, P. A. Wender, Organ- and cell-selective delivery of mRNA in vivo using guanidinylated serinol charge-altering releasable transporters, J. Am. Chem. Soc. 146 (2024) 14785–14798, https://doi.org/10.1021/jacs.4c02704.
[28] J. Yum, B.S. Kim, S. Ogura, R. Kamegawa, M. Naito, Y. Yamasaki, H.J. Kim, K. Miyata, Fine-tuning of polyaspartamide derivatives with alicyclic moieties for systemic mRNA delivery, J. Contr. Release 342 (2022) 148–156, https://doi.org/10.1016/j.jconrel.2021.12.040.
[29] X. Yu, S. Liu, Q. Cheng, S.M. Lee, T. Wei, D. Zhang, L. Farbiak, L.T. Johnson, X. Wang, D.J. Siegwart, Hydrophobic optimization of functional poly(TPAE-co-suberoyl chloride) for extrahepatic mRNA delivery following intravenous administration, Pharmaceutics 13 (2021) 1914, https://doi.org/10.3390/pharmaceutics13111914.
[30] A.M. Vargason, A.C. Anselmo, S. Mitragotri, The evolution of commercial drug delivery technologies, Nat. Biomed. Eng. 5 (2021) 951–967, https://doi.org/10.1038/s41551-021-00698-w.
[31] S. Shaha, D. Rodrigues, S. Mitragotri, Locoregional drug delivery for cancer therapy: preclinical progress and clinical translation, J. Contr. Release 367 (2024) 737–767, https://doi.org/10.1016/j.jconrel.2024.01.072.
[32] H. Shin, S. Kang, C. Won, D.H. Min, Enhanced local delivery of engineered IL-2 mRNA by porous silica nanoparticles to promote effective antitumor immunity, ACS Nano 17 (2023) 17554–17567, https://doi.org/10.1021/acsnano.3c06733.
[33] S.Y. Neshat, C.H.R. Chan, J. Harris, O.M. Zmily, S. Est-Witte, J. Karlsson, S. R. Shannon, M. Jain, J.C. Doloff, J.J. Green, S.Y. Tzeng, Polymeric nanoparticle gel for intracellular mRNA delivery and immunological reprogramming of tumors, Biomaterials 300 (2023) 122185, https://doi.org/10.1016/j.biomaterials.2023.122185.
[34] Z. Song, Z. Han, S. Lv, C. Chen, L. Chen, L. Yin, J. Cheng, Synthetic polypeptides: from polymer design to supramolecular assembly and biomedical application, Chem. Soc. Rev. 46 (2017) 6570–6599, https://doi.org/10.1039/C7CS00460E.
[35] H. Cabral, K. Miyata, K. Osada, K. Kataoka, Block copolymer micelles in nanomedicine applications, Chem. Rev. 118 (2018) 6844–6892, https://doi.org/10.1021/acs.chemrev.8b00199.
[36] Y. Zhang, P. He, P. Zhang, X. Yi, C.S. Xiao, X.S. Chen, Polypeptides-drug conjugates for anticancer therapy, Adv. Healthcare Mater. 10 (2021) 2001974, https://doi.org/10.1002/adhm.202001974.
[37] C. Deng, Q. Zhang, J. Guo, X. Zhao, Z. Zhong, Robust and smart polypeptide-based nanomedicines for targeted tumor therapy, Adv. Drug Deliv. Rev. 160 (2020) 199–211, https://doi.org/10.1016/j.addr.2020.10.019.
[38] Y. Mochida, H. Cabral, Y. Miura, F. Albertini, S. Fukushima, K. Osada, N. Nishiyama, K. Kataoka, Bundled assembly of helical nanostructures in polymeric micelles loaded with platinum drugs enhancing therapeutic efficiency against pancreatic tumor, ACS Nano 8 (2014) 6724–6738, https://doi.org/10.1021/nn500498t.
[39] H.J. Kim, S. Ogura, T. Otabe, R. Kamegawa, M. Sato, K. Kataoka, K. Miyata, Fine-tuning of hydrophobicity in amphiphilic polyaspartamide derivatives for rapid and transient expression of messenger RNA directed toward genome engineering in brain, ACS Cent. Sci. 5 (2019) 1866–1875, https://doi.org/10.1021/acscentsci.9b00843.
[40] N.L. Benner, R.L. McClellan, C.R. Turlington, O.A.W. Haabeth, R.M. Waymouth, P. A. Wender, Oligo(serine ester) charge-altering releasable transporters: organocatalytic ring-opening polymerization and their use for in vitro and in vivo mRNA delivery, J. Am. Chem. Soc. 141 (2019) 8416–8421, https://doi.org/10.1021/jacs.9b03154.
[41] P. Zhao, X. Hou, J. Yan, S. Du, Y. Xue, W. Li, G. Xiang, Y. Dong, Long-term storage of lipid-like nanoparticles for mRNA delivery, Bioact. Mater. 5 (2020) 358–363, https://doi.org/10.1016/j.bioactmat.2020.03.001.
[42] W. Shen, H. Wang, Y. Ling-Hu, J. Lv, H. Chang, Y. Cheng, Screening of efficient polymers for siRNA delivery in a library of hydrophobically modified polyethyleneimines, J. Mater. Chem. B 4 (2016) 6468–6474, https://doi.org/10.1039/c6tb01929c.
[43] S. Wannasarit, S. Wang, P. Figueiredo, C. Trujillo, F. Eburnea, L. Simon-Gracia, A. Correia, Y. Ding, T. Teesalu, D. Liu, R. Wiwattanapatapee, H.A. Santos, W. Li, A virus-mimicking pH-responsive acetalated dextran-based membrane-active polymeric nanoparticle for intracellular delivery of antitumor therapeutics, Adv. Funct. Mater. 29 (2019) 1905352, https://doi.org/10.1002/adfm.201905352.
[44] C. Li, J. Zhou, Y. Wu, Y. Dong, L. Du, T. Yang, Y. Wang, S. Guo, M. Zhang, A. Hussain, H. Xiao, Y. Weng, Y. Huang, X. Wang, Z. Liang, H. Cao, Y. Zhao, X. Liang, A. Dong, Y. Huang, Core role of hydrophobic core of polymeric nanomicelle in endosomal escape of siRNA, Nano Lett. 21 (2021) 3680–3689, https://doi.org/10.1021/acs.nanolett.0c04468.
[45] P. Kanjilal, K. Dutta, S. Thayumanavan, Thiol-disulfide exchange as a route for endosomal escape of polymeric nanoparticles, Angew. Chem. Int. Ed. 61 (2022) 1433–7851, https://doi.org/10.1002/anie.202209227.
[46] H. Fang, Z. Guo, L. Lin, J. Chen, P. Sun, J. Wu, C. Xu, H. Tian, X. Chen, Molecular strings significantly improved the gene transfection efficiency of polycations, J. Am. Chem. Soc. 140 (2018) 11992–12000, https://doi.org/10.1021/jacs.8b05341.
[47] S.L. Hewitt, D. Bailey, J. Zielinski, A. Apte, F. Musenge, R. Karp, S. Burke, F. Garcon, A. Mishra, S. Gurumurthy, A. Watkins, K. Arnold, J. Moynihan, E. Clancy-Thompson, K. Mulgrew, G. Adjei, K. Deschler, D. Potz, G. Moody, D. A. Leinster, S. Novick, M. Sulikowski, C. Bagnall, P. Martin, J.M. Lapointe, H. Si, C. Morehouse, M. Sedic, R.W. Wilkinson, R. Herbst, J.P. Frederick, N. Luheshi, Intratumoral IL12 mRNA therapy promotes TH1 transformation of the tumor microenvironment, Clin. Cancer Res. 26 (2020) 6284–6298, https://doi.org/10.1158/1078-0432.CCR-20-0472.
[48] L.N.M. Nguyen, Z.P. Lin, S. Sindhwani, P. MacMillan, S.M. Mladjenovic, B. Stordy, W. Ngo, W.C.W. Chan, The exit of nanoparticles from solid tumours, Nat. Mater. 22 (2023) 1261–1272, https://doi.org/10.1038/s41563-023-01630-0.
[49] D. Xue, B. Moon, J. Liao, J. Guo, Z. Zou, Y. Han, S. Cao, Y. Wang, Y.-X. Fu, H. Peng, A tumor-specific pro-IL-12 activates preexisting cytotoxic T cells to control established tumors, Sci. Immunol. 7 (2022) eabi6899, https://doi.org/10.1126/sciimmunol.abi6899.
[50] B. Mirlekar, Y. Pylayeva-Gupta, IL-12 family cytokines in cancer and immunotherapy, Cancers 13 (2021) 167, https://doi.org/10.3390/cancers13020167.
[51] S. Chen, X. Huang, Y. Xue, E. Álvarez-Benedicto, Y. Shi, W. Chen, S. Koo, D. J. Siegwart, Y. Dong, W. Tao, Nanotechnology-based mRNA vaccines, Nat. Rev. Methods Primers 3 (2023) 1027–1037, https://doi.org/10.1038/s43586-023-00246-7.
[52] James C. Kaczmarek, A. K. P, Luke H. Rhym, Umberto Capasso Palmiero, Balkrishen Bhat e, Michael W. Heartlein, Frank DeRosa, Daniel G. Anderson, Systemic delivery of mRNA and DNA to the lung using polymer-lipid nanoparticles, Biomaterials 275 (2021) 120966, https://doi.org/10.1016/j.biomaterials.2021.120966.
[53] S. Luozhong, Z. Yuan, T. Sarmiento, Y. Chen, W. Gu, C. McCurdy, W. Gao, R. Li, S. Wilkens, S. Jiang, Phosphatidylserine lipid nanoparticles promote systemic RNA delivery to secondary lymphoid organs, Nano Lett. 22 (2022) 8304–8311, https://doi.org/10.1021/acs.nanolett.2c03234.
[54] R. Zhang, S. Shao, Y. Piao, J. Xiang, X. Wei, Z. Zhang, Z. Zhou, J. Tang, N. Qiu, X. Xu, Y. Liu, Y. Shen, Esterase-labile quaternium lipidoid enabling improved mRNA-LNP stability and spleen-selective mRNA transfection, Adv. Mater. 35 (2023) e2303614, https://doi.org/10.1002/adma.202303614.
[55] L.N.M. Nguyen, Z.P. Lin, S. Sindhwani, P. MacMillan, S.M. Mladjenovic, B. Stordy, W. Ngo, W.C.W. Chan, The exit of nanoparticles from solid tumours, Nat. Mater. 22 (2023) 1261–1272, https://doi.org/10.1038/s41563-023-01630-0.
[56] D.J. Propper, F.R. Balkwill, Harnessing cytokines and chemokines for cancer therapy, Nat. Rev. Clin. Oncol. 19 (2022) 237–253, https://doi.org/10.1038/s41571-021-00588-9.
[57] C.S. Garris, S.P. Arlauckas, R.H. Kohler, M.P. Trefny, S. Garren, C. Piot, C. Engblom, C. Pfirschke, M. Siwicki, J. Gungabeesoon, G.J. Freeman, S.E. Warren, S. Ong, E. Browning, C.G. Twitty, R.H. Pierce, M.H. Le, A.P. Algazi, A.I. Daud, S. I. Pai, A. Zippelius, R. Weissleder, M.J. Pittet, Successful anti-PD-1 cancer immunotherapy requires T cell-dendritic cell crosstalk involving the cytokines IFN-gamma and IL-12, Immunity 49 (2018) 1148–1161, https://doi.org/10.1016/j.immuni.2018.09.024.